Athermalized low-loss echelle-grating-based multimode dense wavelength division demultiplexer

Jie Qiao, Feng Zhao, Ray T. Chen, James W. Horwitz, and William W. Morey

A high-density wavelength division demultiplexer (DEMUX) capable of demultiplexing eight-channel 200-GHz optically spaced signals into a 62.5-μm multimode-fiber array is reported. The wavelength range of operation is from 1549.32 to 1560.61 nm within the International Telecommunication Union grid. The measured wavelength accuracy is within 0.04 nm. The mean insertion loss of this DEMUX is 1.95 dB. Thermal analysis and temperature testing results are reported. The temperature test cycling from 20 °C to 60 °C indicates that the wavelength thermal drift is less than 0.8 pm/°C. Adjacent cross talk is measured to be better than −45 dB. The measured data transmission bit rate of this device is higher than 3.5 Gb/s. © 2002 Optical Society of America

OCIS codes: 060.2340, 060.1810, 230.1950, 260.2030, 090.1970, 120.4570.

1. Introduction

Owing to the explosive demand for high-bandwidth applications and the accompanying short distance, multimode dense wavelength division multiplexing (DWDM) has become an essential, robust, and high-performance data- and air-link technology in metropolitan area networks (MANs) and local area networks (LANs).[1–7] Multimode fiber represents the sizable portion of the fibers used in LANs, owing to its low-cost installation and maintenance. It was installed in LANs as early as the 1980's.[8] Wavelength division multiplexing (WDM) has been a cost-effective method of increasing the capacity of long-haul fiber links. But the WDM for data communications has to be quite low cost, compact, and compatible with multimode fiber. The potential for a large number of closely spaced channels and the inherent advantage of compactness make bulk diffraction grating-based demultiplexers (DEMUXs) quite attractive for multimode DWDM applications.[9,10] Meanwhile, there is also an urgent need to find solutions to overcome the temperature dependence in multimode DEMUXs, to broaden the optical passband, and to decrease the cost and the device size. In this paper we present an athermalized passband-broadened DEMUX with low insertion loss and low cross talk for MANs and LANs.

2. High-Order Echelle Grating's Design Principle and Parameters

A high-order echelle grating has several special properties that make it an excellent diffraction component for WDM diffraction. Most apparent is its high dispersion, which permits compact optical systems with a high throughput and high resolution. In addition, because it is never used far from the blaze direction, the grating efficiency remains relatively high over a large spectral range. Furthermore, when the grating is operated at higher orders, it is nearly free of the polarization effect. Under the Littrow mount condition, when the incident angle is the same as the diffraction angle, another useful property comes into play: One lens can collimate and focus simultaneously, resulting in lower cost and decreased packaging size for the WDM system.

A. Calculation of the Desired Diffraction Order

Usually, the higher the grating order, the smaller the polarization effect of the grating. But any given grating order is also limited by certain factors. One

When this research was performed, J. Qiao, F. Zhao, and R. T. Chen (raychen@uts.cc.utexas.edu) were with the Microelectronics Research Center, the Department of Electrical and Computer Engineering, The University of Texas at Austin, Austin, Texas 78758. J. Qiao (jie@alumni.utexas.net) is now with LNL Technologies, One Broadway, 14th Floor, Cambridge, Massachusetts 02139. J. W. Horwitz and W. W. Morey were with Radiant Photonics Incorporated, 12100 Technology Boulevard, Austin, Texas 78727. J. W. Horwitz is now with Raytheon Santa Barbara Remote Sensing, 75 Coromar Drive, Goleta, California 93117. W. M. Morey is now with Sabeus Photonics, Inc., 20630 Nordhoff Street, Chatsworth, California 91311.

Received 19 March 2002; revised manuscript received 3 July 2002.

0003-6935/02/316567-09$15.00/0

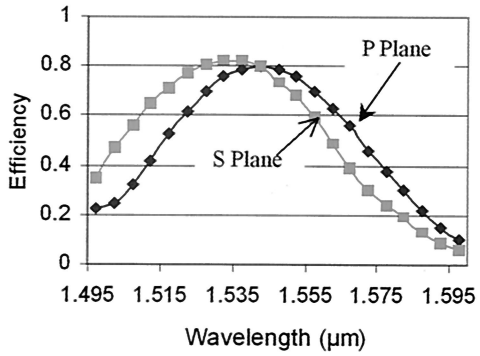

Fig. 1. Diffraction efficiency of the 22nd echelle grating.

of them is the working spectral range. We calculated the corresponding grating working order to cover the C band's spectral range (from 1528 to 1560 nm). When the extremes of the C band are represented by $\lambda_1 = 1528$ nm and $\lambda_2 = 1560$ nm, the formula for calculating the grating order for a certain spectrum range can be expressed as[11]:

$$m = \frac{\lambda_1}{\lambda_2 - \lambda_1}. \tag{1}$$

So that the spectrum of the C band signal λ_2, operating at m order, does not overlap the spectrum of signal λ_1, when operating at $m + 1$ order, m must be less than 47. However, we must leave room to fully reduce the noise caused by the scattering of adjacent orders.

We chose 22 as the grating working order, and the grating groove spacing (19 μm) is large compared with the wavelength (1.5 μm). This in turn implies that the scalar theory of diffraction may be used. Each groove facet is a small mirror or a small prism that behaves in the same way as a large one. However, when the widths of the grooves are comparable with the wavelength of light, this assumption is no longer valid because the oscillations of the electrons are impeded or curtailed by the boundary of the facet. In practice, when the groove spacing is less than approximately three times the wavelength, the efficiency curves for the two polarizations differ dramatically, and the blaze wavelengths differ.[11] Figure 1 shows our measurements of the grating efficiency across all working wavelengths. The grating efficiency varies from 61%–75% within the whole working wavelength range (1549.32–1560.61 nm). By use of a 22nd-order grating, the diffraction efficiency is almost independent of the polarization of incident light.

B. Diffraction Angle and Angular Dispersion Calculation

The reflection grating's diffraction equation is[12]

$$n\Lambda(\sin\theta_i + \sin\theta_d) = m\lambda, \tag{2}$$

where θ_i is the incident angle, θ_d is the diffraction angle, and θ_i and θ_d are measured from the grating normal; m is the order of diffraction; λ is the wavelength; Λ is the groove spacing; and n is the refraction index of the medium containing the incident and diffracted rays. Here $n = 1$. We found the angular dispersion by taking the first-order derivative of θ_d:

$$\frac{d\theta_d}{d\lambda} = \frac{\sin\theta_i + \sin\theta_d}{\lambda\cos\theta_d}. \tag{3}$$

For the Littrow condition $\theta_i = \theta_d$, and the angular dispersion is

$$\frac{d\theta_d}{d\lambda} = \frac{2\tan\theta_d}{\lambda}. \tag{4}$$

The larger the diffraction angle, the greater the angular dispersion. In our design of the eight-channel DEMUX the angular dispersion of the grating at the central wavelength ($\lambda = 1555.32$ nm) was 2.62 mrad/nm.

A blazed grating redirects the incident light in the direction of a chosen diffracted order if each groove is formed appropriately. Thus in a reflection grating each groove consists of a small mirror inclined at an appropriate angle. The blaze condition is satisfied when the angle of incidence with respect to the facet normal is equal to the angle of reflection from the facet; if the facet angle is ϕ, then

$$\theta_i - \phi = \theta_d + \phi; \tag{5}$$

$$\phi = \frac{\theta_i - \theta_d}{2} \quad \text{or} \quad \theta_d = \theta_i - 2\phi. \tag{6}$$

Considering the Littrow mount, $\theta_i = -\theta_d$, so $\phi = \theta_d$, which is the situation depicted in Fig. 2. The grating blaze angle was 64°.

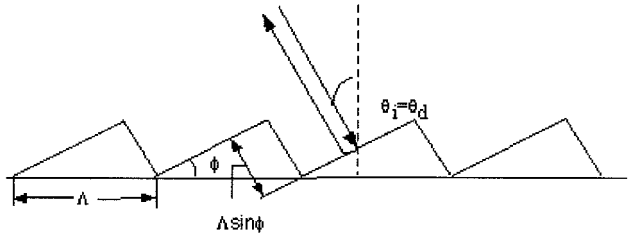

Fig. 2. Blazed grating used in the Littrow mounting.

3. Device Configuration and Optical Design Details

The device was designed to have eight channel outputs and to be operated in the frequency region from 192.1 to 193.5 THz (wavelength from 1548.90–1560.19 nm) within the International Telecommunication Union grid. The channel spacing is 200 GHz. Figure 3 shows a schematic diagram of this device. The input optical signals coming from a tunable external-cavity semiconductor laser passed through 1-km of coiled multimode fiber, which was used as a mode scrambler. The source was then introduced into the DEMUX through the input channel of a silicon V-grooved multimode-fiber array. This 62.5–125-μm multimode-fiber array has one input fiber

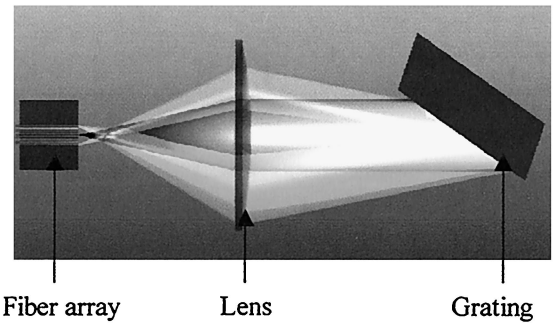

Fig. 3. Geometrical layout of the eight-channel multimode DEMUX.

and eight output fibers placed in a single-layer silicon V-groove chip, which was designed to have variable fiber spacing because of the nonlinear effect of the angular dispersion. An optimized diffraction-limited triplet lens was used to collimate the incident light from the inputs and to focus the diffracted lights from the grating into the corresponding fiber array channels.

The grating was operated in a high diffraction order to minimize the polarization-dependent loss. The grating operates at large angles of incidence and diffraction so as to provide large angular dispersion. The large dispersion reduces the focal length of the lens and hence the size of the instrument.

The 62.5-μm multimode fiber has a numerical aperture of 0.275, requiring the use of a lens large enough to accept and collect light with this numerical aperture across the entire fiber array. Figure 4 shows a cross section of the optics of the eight-channel DEMUX. The vertical line at the left of this figure is the focal plane, and the front end of the fiber array (not shown) is in this plane. Light leaves the input fiber and is collimated by the lens. The grating gives an angular dispersion of the light into its constituent frequencies, the rays of one of which are shown in the diagram. The light for this frequency, 192.1 THz, is focused by the lens onto an output fiber. For simplicity, rays for the other seven channels are not shown.

The lens is telecentric. That is, the input beam and all output beams are parallel to the optical axis. This fact has important consequences. First, insertion loss is minimized because all the output beams are perpendicular to their respective fibers. Second, the frequency of a channel is invariant with respect to changes in focus. Because there are small changes in focus with changes in temperature, the frequency will not be a function of temperature. The experimental data below confirmed this fact.

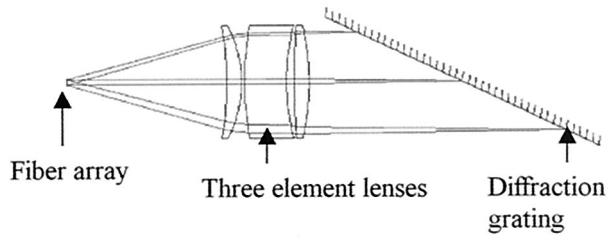

Fig. 4. Cross section of the optics of the eight-channel DEMUX.

The focal length f of the lens can be calculated by Eq. (7) once the fiber spacing Δy and wavelength increment $\Delta\lambda$ between adjacent channels is known:

$$f = \frac{\Delta y}{\Delta\lambda}\frac{\lambda}{2\tan\theta_d}. \tag{7}$$

The above formula shows that the focal length of the lens is directly proportional to the fiber spacing and to the tangent of the angle of diffraction. Thus, to make the lens small, one can use closely spaced fibers and a large diffraction angle.

4. Thermal Stability Analysis and Compensation

The most challenging part in optical multiplexer (MUX)–DEMUX design is to meet the reliability and performance criteria over a wide operating temperature. Power consumption to operate the optical networks increases with the growing complexities of networks, so passive athermalized optical MUXs–DEMUXs that do not use any external temperature controllers are highly desirable.

When temperature changes, the insertion loss and the center wavelength may change accordingly. The center wavelength shift is caused mainly by the change of groove spacing of the grating. The change of insertion loss is due to the thermal variation in lens focal length, and the image shift in the vertical direction is caused by the difference of the thermal coefficient of expansion (TCE) of the lens and its supporting material. We will show in this section that it is possible to eliminate or reduce the thermal effect by careful optical design, which includes choosing the correct materials for making the grating, lens, and housing.

A. Central Wavelength Shift of Individual Channels

The thermal expansion of the grating can be calculated by Eq. (8):

$$\Lambda = \Lambda_0(1 + \beta\Delta T), \tag{8}$$

where β is the TCE of the grating and ΔT is the change of temperature. Assuming that the incident and diffraction angles keep constant with temperature and combining the temperature derivatives of Eqs. (2) and (8), we can easily find the wavelength shift caused by temperature:

$$\Delta\lambda = \beta\lambda\Delta T. \tag{9}$$

When temperature changes within a certain range, the larger the TCE of the grating, the greater the shift of the center wavelength. The grating we employed has ultralow TCE. The TCE is zero from 0 °C to 35 °C and less than 0.06×10^{-6}/°C when the temperature is higher than 35 °C (which is 1180 times less than the TCE of BK-7, which is 7.1×10^{-6}/K).[13] When $\lambda = 1550$ nm, the temperature

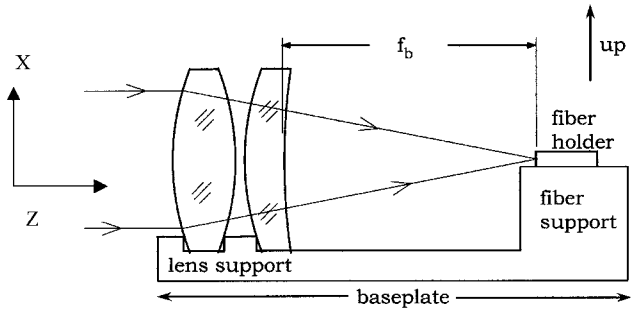

Fig. 5. Simplified cross-sectional view of the section of a DEMUX that includes the lens and the fiber holder.

changes from 20 °C to 60 °C ($\Delta T = 40$ °C), and $\Delta\lambda = 0.037$ nm. The experiment results in Section 6 also proved that deploying an ultralow expansion grating suppressed the wavelength shift successfully.

B. Insertion Loss Shift

The shift of insertion loss with temperature variation is mainly due to the change of lens focal length and vertical and lateral image shift.

1. Changes in Lens Focus

We analyzed the thermal performance of the lens shown in Fig. 4 and found that its focus relative to the end of the fiber mount varied with temperature. With reference to Fig. 5, the change in back focal length Δf_b that is due to a change in temperature ΔT must be equal and opposite to the change in length Δz_m of the portion of the baseplate that lies between the lens and the fiber mount. That is,

$$\Delta f_b = -\Delta z_m. \tag{10}$$

To correctly calculate thermal changes in the DWDM, one must consider thermal changes in the refractive index of each lens element, the thermal expansion of the lens elements, the thermal expansion of the spacers between the optical parts, and the thermal expansion of the grating period. All these parameters were handled by the optical design software (ZEMAX) that we used, so that we were able to accurately simulate thermal changes of back focal length and overall optical performance.

Because available optical glasses have wide variations in the first derivative of the refractive index with respect to temperature, one is able to select a glass or glasses for the lens elements that not only will satisfy Eq. (10) for a chosen baseplate material but will also provide an opportunity for the lens to be aberration corrected over the entire temperature range. That is, we have been able to fully optimize our lenses to have athermal performance, with consideration of the effect of expansion in the lens spacers and the mount. This is a considerable improvement, compared with the conventional approach of merely keeping the effective focal length or the back focal length constant.

2. Image Shift in the Vertical Direction

The image shift in the vertical direction can be expressed as

$$\Delta x = \tfrac{1}{2} D \Delta T (\beta_L - \beta_M), \tag{11}$$

where D is the diameter of the lens, ΔT is the change of temperature, and β_L and β_M are the TCEs of the lens and its supporting parts. Equation (11) indicates that, when the temperature changes within a certain degree, the better the TCEs of the lens and its supporting materials are matched, the smaller the image shift and then the smaller the insertion loss shift. The differential expansion in the vertical direction is directly proportional to the lens diameter, so that thermal problems become severe for large lenses unless the expansion coefficients of the lens elements are nearly equal to each other and to those of the support. For the eight-channel multimode DWDM ($D = 39.6$ mm), the image shift is 0.16 μm, which can be ignored in view of the multimode-fiber core diameter (62.5 μm).

3. Image Shift in the Dispersion Direction

Because the WDM system is symmetric in the lateral direction, the image shift in the lateral direction is mainly caused by the change in the central wavelength. The lateral image shift Δy can be expressed as

$$\Delta y = \frac{2\Delta\lambda \tan \theta_{\text{diff}} f}{\lambda}, \tag{12}$$

where $\Delta\lambda$ is the shift of the working wavelength caused by temperature variation. Combining Eqs. (9) and (12), we can easily obtain the relation between the lateral image shift and the TCE of the grating material and temperature change:

$$\Delta y = 2\beta \Delta T f \tan \theta_{\text{diff}}. \tag{13}$$

It is obvious that the larger the diffraction angle or the larger the TCE of the grating material, the greater the lateral image shift with temperature. In our design, the lateral image shift was suppressed to 0.06 μm. It is ignorable, considering the large core size of the multimode fiber.

The optical performance of the DEMUX reported in this paper was diffraction limited at all wavelengths and invariant with temperature. We expect this design to have no observable changes in insertion loss with temperature, provided that the alignment is perfect. The conclusions obtained in this section were based on the assumption that the alignment is perfect. A DWDM can give excellent performance at room temperature but still be misaligned. This misalignment can cause significant changes in signal as the temperature changes. Thus it may be necessary to check that, at room temperature, an alignment parameter is near the center of its range, not merely within its range.

5. Improvement of the Optical Passband

Broadening and flattening of the passband in WDM is a key to maximizing spectral efficiency and relaxing the tolerance on wavelength control in the networks.[14] Typical grating-based WDMs have passbands or spectral responses that are generally highly peaked with a slow roll-off in their wavelength response. This effect results from the diffraction response of the associated grating element that separates the wavelengths, from the transmission response of intervening optical lens elements, and from the receiving optics. Such responses do not use the full bandwidth of most MUXs and DEMUXs. As a result, it is often difficult to specify wavelength tolerances for associated components such as laser light sources, amplifiers, and other optical components.

The width of the optical passband is mainly determined by the filling ratio F, i.e., the ratio of the receiving fiber core diameter to the distance between the centers of two neighbor fibers. The larger this ratio, the larger the passband. To increase the passband, one can either increase the core diameter or decrease the central spacing between adjacent output fibers. The output image reshaping and broadening approach[15,16] has been used for arrayed-waveguide-based WDMs. For diffraction-grating-based WDMs, to increase the core diameter or to increase the mode field diameter, one can use thermal expanded core fibers,[17,18] use graded-index lensed fibers,[19–22] or defocus the focused beam spots at the focal plane.[23] To decrease the fiber spacing, one can strip the coating, etch the cladding to the smallest allowable size, or use a waveguide-concentrator structure. But one can neither increase the core diameter nor decrease the channel spacing without limitation. There is an intrinsic trade-off between passbands and cross talks. A lower cross talk implies a wider separation between the output fibers and, therefore, necessarily higher linear dispersion, resulting in proportional bandwidth narrowing.

The Littrow mount geometry of our WDM design provided aberration-free image systems. The light spots of diffracted beams are almost identical in size to the cores of the fibers. In this case, the optimized value of this ratio is $F = 0.667$.[24]

To increase the optical passband, we inserted a specially designed optical element for expanding the mode field diameter of output light spots into the optical system showed in Fig. 4. The detailed optical design will be reported in a future publication. The typical 3-dB passband was increased from 0.6 to 0.94 nm.[9] The average 1-dB passband was increased from 0.3 to 0.58 nm.

6. Device Performance

The MUX was fabricated as a stand-alone unit. The entire assembling and packaging process is passive and epoxy free so that the possible wavelength and insertion loss shifting caused by the UV curing of epoxy is avoided. Figure 6 shows the inside of the fully packaged eight-channel multimode DEMUX. By improving the mechanical design, by careful choices of optical materials, by employing the epoxy-free packaging and sealed package housing, we have obtained excellent thermal behavior for this DEMUX, from the viewpoint of insertion loss, as well as center wavelength accuracy.

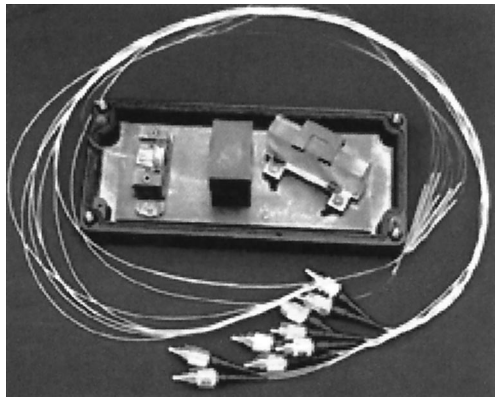

Fig. 6. Inside of the fully packaged eight-channel multimode-in, multimode-out DEMUX.

We measured the transmission spectrum using an amplified spontaneous emission light source and an optical spectrum analyzer having a 0.01-nm resolution. All the measurement results were obtained after the average of three sets of the input and output signals were taken. The insertion losses were measured at the wavelength of minimum loss, which was always within 0.04 nm of the nominal channel center wavelength. The lowest insertion loss for any channel was 1.50 dB; all the channels showed a loss under 2.70 dB with a mean figure of 1.95 dB, which includes the connector loss. Of the 1.95 dB, 1.55 dB is due to the grating diffracting 70% of incident power into the desired diffraction order, 0.1 dB is caused by lens transmission and reflection loss, and the other 0.3 dB is caused by fiber array coupling and connection loss.

We also monitored the change in insertion loss and center wavelength when increasing the operating temperature from 20 °C to 60 °C. The average insertion loss changed from 1.95 to 2.34 dB, which gave a 0.00975 dB/°C loss shift. Figure 7 shows the loss variation against different channels at 20 °C and 60 °C. We could then find that the maximum change in the eight channels was a loss of 1.1 dB, which was within the loss deviation range of 1.2 dB for different channels at room temperature. The average wavelength shift with temperature is 0.8 pm/°C.

The wavelength temperature dependence was successfully suppressed within 0.032 nm in the 20 °C to 60 °C temperature ranges, which is also within the wavelength accuracy range at room temperature. The detailed measured device parameters are listed in Table 1. The wavelength accuracy is within 0.04 nm in the worst case, which was due to the imperfect positions of fibers in the array and the output power shifting of the white-band amplified spontaneous emission light source.

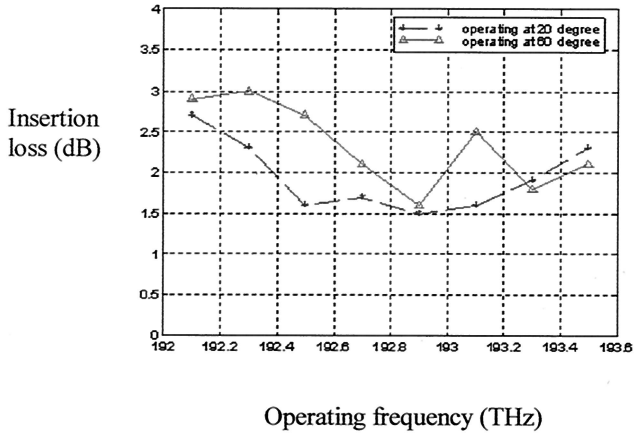

Fig. 7. Insertion loss variation plotted against channel frequency at 20 °C and 60 °C.

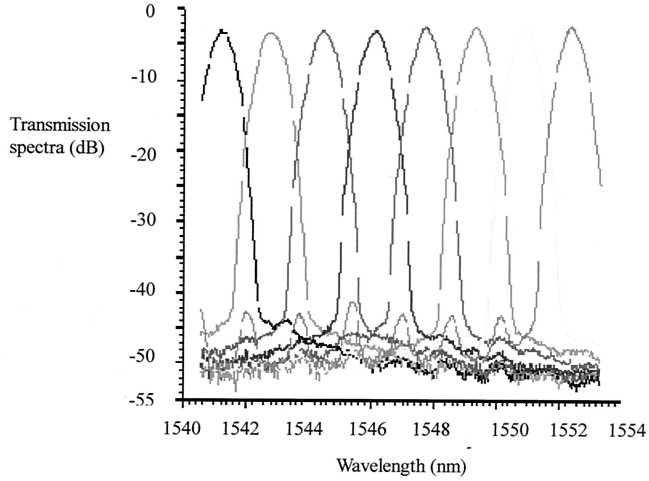

Fig. 8. Output spectrum of a passband-broadened DEMUX.

The device has fairly good isolation; the average adjacent cross talk is 46.5 dB. The typical polarization-dependence loss was measured to be 0.13 dB. Figure 8 shows the output spectrum of a 200-GHz-spaced passband-broadened DEMUX operating at a wavelength range from 1541.35 to 1552.52 nm. The typical 1- and 3-dB passbands are 0.58 and 0.94 nm, respectively.

The main advantage of our approach is simple and cost effective. We achieved an excellent polarization-dependent loss (0.13 dB) by using a high-order echelle grating. This eliminates the need for a polarization splitter and a half-wave plate, as reported by Chassagne *et al.*[25] The athermalized bulk grating-based MUX–DEMUX has advantages over etched grating-based MUXs–DEMUXs by use of an active temperature control unit[26] in that the temperature control unit requires electronic control circuits and a total power consumption of a few watts. Our approach reduces optical system complications and costs and eliminates possible failures caused by electronics. Compared with the most recently reported athermal arrayed-waveguide-grating-based MUXs–DEMUXs[27,28] there were no extra loss and extra phase errors. We also demonstrated improved performance in terms of insertion loss and cross talk compared with results recently reported.[25,26,29]

7. High Data Transmission Bit Rate

To achieve a high data transmitting bit rate in the telecommunications field is the goal of WDM technology. The maximum bit rates are determined by numerous factors, including the signal modulation rate, the transmission bandwidth through the transmission media, and the response time of the optoelectronic devices. In a communications network, the WDM system is simply one part of the transmission regime. The pulse broadening of grating-based DWDM imposes inherent limitations on the data transmission bit rate. We need to optimize the WDM design to decrease pulse broadening caused by gratings, which can be calculated by the formula

$$\Delta\tau_g = \frac{n_0 f \tan(\mathrm{NA})\tan(\theta_d)}{2c}, \tag{14}$$

where the intensity of input light possesses a Gaussian distribution, n_0 is the refractive index of the media in which light is transmitted, c is the speed of light at vacuum, NA = 0.275 is the numerical aperture of the input fiber, the focal length of the lens is $f = 36.9$ mm, and $\theta_d = 63.86$ is the diffraction angle of the grating. So the pulse broadening caused by the grating is $\Delta\tau_g = 3.4 \times 10^{-11}$ s. Equation (14) clearly shows that, when working at a certain wavelength, pulse broadening caused by gratings is proportional to the numerical aperture of the input fiber, to the focal length of the lens, and to the diffraction angle of the grating.

Mode dispersion is another major factor causing pulse broadening in multimode DWDM. For

Table 1. Device Parameters of the Multimode Demultiplexer

Parameters	Channel Number							
	Ch #1	Ch #2	Ch #3	Ch #4	Ch #5	Ch #6	Ch #7	Ch #8
Designed center wavelength (nm)	1560.61	1558.98	1557.36	1555.75	1554.13	1552.52	1550.92	1549.32
Wavelength error at 20 °C (nm)	0.02	0.02	0.04	0	0.02	0.01	0	0.02
Wavelength error at 60 °C (nm)	0.02	0.04	0.008	0.008	0.016	0.032	0.032	0.024
Insertion loss (db)	2.7	2.3	1.6	1.7	1.5	1.6	1.9	2.3
Cross talk (db)	47.8	47.6	48	48	46	45.7	44.6	44.4

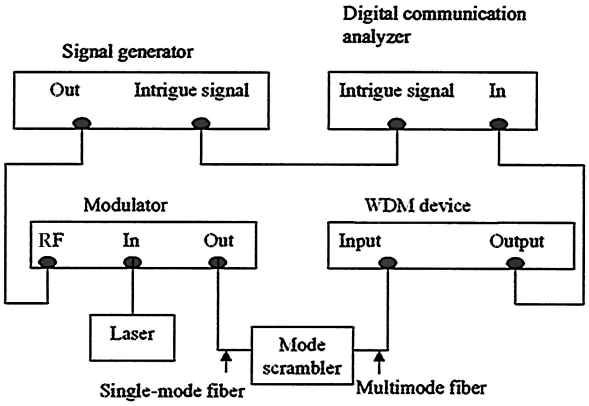

Fig. 9. Experimental setup for data transmission bit rate testing. RF, radio frequency.

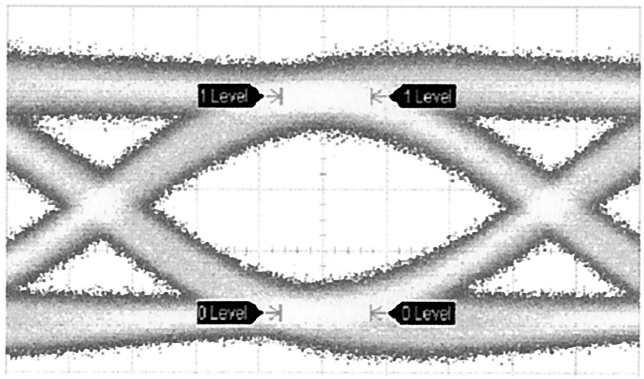

Fig. 10. Experiments confirmed a 3.5-Gb/s data transmission bit rate. The signal-to-noise ratio of the eye diagram was 8.7:1.

graded-index multimode fibers, the pulse broadening can be calculated by Eq. (15):

$$\Delta\tau_m = \frac{Ln_1}{8c}\Delta^2, \tag{15}$$

where the refractive index of the core is $n_1 = 1.473$, the relative index difference is $\Delta = 1.74\%$, the speed of light in the vacuum is $c = 3 \times 10^8$ m/s, and $L = 100$ m is the length of the multimode fiber. The calculated pulse broadening caused by mode dispersion is $\Delta\tau_m = 1.9 \times 10^{-11}$ s. The total pulse broadening can be calculated by Eq. (16):

$$\Delta\tau = (\Delta\tau_g{}^2 + \Delta\tau_m{}^2)^{1/2}. \tag{16}$$

The maximum data transmission bit rate can be expressed as Eq. (17) when the initial pulse width is neglected:

$$\mathrm{BR} = \frac{1}{4\Delta\tau}. \tag{17}$$

Here the total pulse broadening is $\Delta\tau = 4.3 \times 10^{-11}$ s; therefore the theoretical bit rate BR = 5.8 Gb/s. We measured the data transmission bit rate using the setup shown in Fig. 9. The maximum signal speed of the signal generator was 3.5 Gb/s. The random signal from the signal generator at the speed of 3.5 Gb/s was sent to a modulator to modulate the intensity of the optical signal from a tunable laser. The modulated optical signal passed through a mode scrambler and then was sent to the input channel of the WDM device. A digital communication analyzer was used to measure the eye diagram of the output channels. Figure 10 shows a clearly open eye diagram when the input optical signal was modulated at 3.5 Gb/s. The applied current is 120 mA; the ratio of signal to noise is S/N = 8.7.

8. Discussion: Simulation for the Tolerance of Image Shift

Disturbances caused by laser drifting, temperature change, and vibration are reflected as a relative movement of the input light spot at the receiving fiber or as a shifting of wavelength. A larger 1-dB passband is therefore always preferable. To calculate the transverse loss of the WDM system, we assume that the core diameter of the receiving fiber is $D = 2R$ and the diameter of the input light spot is $d = 2r$. We express the ratio of energy in the area of overlap (input light spot and receiving fiber) to energy in the entire area of the input light spot as

$$\eta = \frac{\int_{s'} f'(x, y)\mathrm{d}s'}{\int_{s} f(x, y)\mathrm{d}s}, \tag{18}$$

where η is the ratio of energy, s' is the overlap area, and s is the input light spot area. The optical power distribution function at the overlap area and the whole area of the input light spot are $f'(x, y)$ and $f(x, y)$, respectively. Figure 11 illustrates Eq. (18). We can obtain the maximum tolerance of image shift when the WDM system functions within a 1-dB passband range.

Here we assume a uniform power distribution

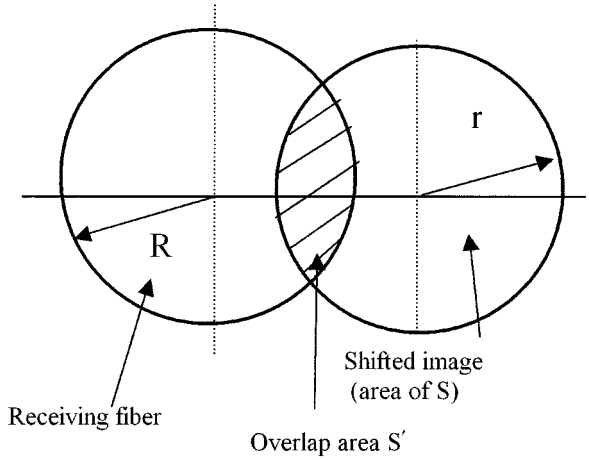

Fig. 11. Illustration of the overlap region of a receiving fiber and the input spot.

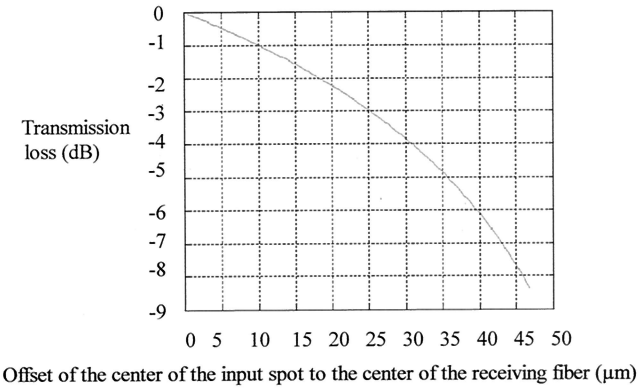

Fig. 12. Simulation result shows ±10-μm image-shift tolerance within 1-dB passband.

across the whole area of the input light spot. We simulated the theoretical 1-dB passband calculation, in which $D = 62.5$ μm and $d = 62.5$ μm. Figure 12 shows the simulation result, which indicates that when a system is diffraction limited, i.e., the input spot size is the same as the multimode-fiber core diameter, the maximum image-shift tolerance can be as much as ±10 μm within a 1-dB passband. This large image-shift tolerance helps the device to resist various kinds of environmental disturbances.

9. Summary

We designed and demonstrated an athemalized grating-based eight-channel DEMUX with high resolution and low insertion loss. This approach improves cost effectiveness and simplicity of optical systems by elimination of the need for an active temperature control unit and polarization compensators. The fully packaged device has 1.95- and 2.34-dB insertion losses at 20 °C and 60 °C, respectively. The mean cross talk is 46.7 dB. To the authors' knowledge, those are the best-reported results for a multimode DWDM. The wavelength accuracy is within 0.04 nm. The 3-dB passband was measured to be 0.94 nm. This low-cost and highly stable DEMUX can be employed for both MANs and LANs.

The contributions of Ray Collins and George Chang on device packaging are gratefully acknowledged. J. Qiao also thanks Xuegong Deng for valuable discussions on high-speed transmissions.

References

1. C. DeCusatis, "Optical data communication: fundamentals and future directions," Opt. Eng. **37,** 3082–3099 (1998).
2. R. R. Patel, H. E. Garrett, M. A. Emanuel, M. C. Larson, M. D. Pocha, D. M. Krol, R. J. Deri, and M. E. Lowry, "WDM filter modules in compact, low-cost plastic packages for byte-wide multimode fiber ribbon cable data links," Electron. Lett. **35,** 840–841 (1999).
3. B. E. Lemoff, L. B. Aronson, and L. A. Buckman, "Zigzag waveguide demultiplexer for multimode WDM LAN," Electron. Lett. **34,** 1014–1016 (1998).
4. L. B. Aronson, B. E. Lemoff, and L. A. Buckman, "Low-cost multimode WDM for local area networks up to 10Gb/s," IEEE Photon. Technol. Lett. **10,** 1489–1491 (1998).
5. S.-Y. Hu, J. Ko, E. R. Hegblom, and L. A. Coldren, "Multimode WDM optical data links with monolithically integrated multiple-channel VCSEL and photodetector arrays," IEEE J. Quantum Electron. **34,** 1403–1414 (1998).
6. M. Koga and T. Matsumoto, "A novel optical WDM demultiplexer consisting of a simple optical multimode guide and an electrical neural network," IEEE Photon. Technol. Lett. **2,** 487–489 (1990).
7. W. J. Tomlinson, "Wavelength multiplexing in multimode optical fibers," Appl. Opt. **16,** 2180–2194 (1977).
8. R. C. Lasky, U. L. Osterberg, and D. P. Stigliani, *Optoelectronics for Data Communications* (Academic, New York, 1995).
9. J. Qiao, F. Zhao, R. T. Chen, W. W. Morey, J. W. Horwitz, R. Collins, G. Chang, and V. Villavicencio, "Multimode 200-GHz-spaced dense wavelength division demultiplexing for local area networks," in *WDM and Photonic Switching Devices for Network Applications II*, R. T. Chen and G. F. Lipscomb, eds., Proc. SPIE **4289,** 52–58 (2001).
10. Y. Kanabar, N. Baker, G. J. Cannell, and A. Robertson, "High density wavelength division multiplexing for multiple access networks," in *IEE Colloquium on Optical Multiple Access Networks* (Institution of Electrical Engineers, London, UK, 1991), pp. 9/1–9/4.
11. M. C. Hutley, *Diffraction Gratings* (Academic, New York, 1982).
12. E. G. Loewen and E. Popov, *Diffraction Gratings and Applications* (Marcel Dekker, New York, 1997).
13. "Schott Optical Glass," Schott Glass Technologies, 400 York Ave., Duryea, Pa. 18642 (1992).
14. E. G. Churin and P. Bayvel, "Passband flattening and broadening techniques for high spectral efficiency wavelength demultiplexers," Electron. Lett. **35,** 27–28 (1999).
15. C. Dragone, T. Strasser, G. A. Bogert, L. W. Stulz, and P. Chou, "Waveguide grating router with maximally flat passband produced by spatial filtering," Electron. Lett. **33,** 1312–1314 (1997).
16. A. Rigny, A. Bruno, and H. Sik, "Multigrating method for flattened spectral response wavelength multi/demultiplexer," Electron. Lett. **33,** 1701–1702 (1997).
17. C. P. Botham, "Theory of tapering single-mode optical fibres by controlled core diffusion," Electron. Lett. **24,** 243–244 (1988).
18. J. S. Harper, C. P. Botham, and S. Hornung, "Tapers in single-mode optical fibre by controlled core diffusion," Electron. Lett. **24,** 245–246 (1988).
19. D. T. Moore, "Gradient-index optics: a review," Appl. Opt. **19,** 1035–1043 (1980).
20. K. Shiraishi, A. Ogura, and K. Matsuura, "Spotsize contraction in standard single-mode fibers by use of a GI-fiber tip with a high focusing parameter," IEEE Photon. Technol. Lett. **10,** 1757–1759 (1998).
21. W. Bludau and R. Rossberg, "Low-loss laser-to-fiber coupling with negligible optical feedback," J. Lightwave Technol. **LT-3,** 294–302 (1985).
22. K. Shiraishi, "A new lensed-fiber configuration employing cascaded GI-fiber chips," J. Lightwave Technol. **18,** 787–794 (2000).
23. J. Laude and K. Lange, "Dense wavelength division multiplexer and routers using diffraction grating," Proc. NFOEC 99 **1,** 83–88 (1999).
24. J. Hirsh, V. Y. Kalindjian, F. S. Lin, M. R. Wang, G. Xu, and T. Jannson, "High-channel-density broadband wavelength division multiplexers based on periodic grating structures," in *Application and Theory of Periodic Structures*, T. Jannson and N. C. Gallagher, eds., Proc. SPIE **2532,** 171–181 (1995).
25. B. Chassagne, K. Aubry, L. Fulop, and V. Dentan, "Low-loss athermal bulk-optic flat-top passband MUX/DMUX," Electron. Lett. **38,** 235–236 (2002).

26. S. Janz, M. Pearson, B. Lamontagne, L. Erickson, A. Deläge, P. Cheben, D.-X. Xu, M. Gao, A. Balakrishnan, J. Miller, and S. Charbonneau, "Planar waveguide echelle gratings: an embeddable diffractive element for photonic integrated circuits," in *Optical Fiber Communication Conference and Exhibit Technical Digest* (Optical Society of America, Washington, D.C., 2002), pp. 69–70.
27. A. Kaneko, S. Kamei, Y. Inoue, H. Takahashi, and A. Sugita, "Athermal silica-based arrayed-waveguide grating (AWG) multiplexers with new low loss groove design," in *Optical Fiber Communication Conference* (Optical Society of America, Washington, D.C., 1999), pp. Tu01–1–Tu01–3.
28. K. Maru, M. Ohkawa, H. Nounen, S. Takasugi, S. Kashimura, H. Okano, and H. Uetsuka, "Athermal and center wavelength adjustable arrayed-waveguide grating," in *Optical Fiber Communication Conference* (Optical Society of America, Washington, D.C., 2000), pp. 130–132.
29. N. Keil, H. H. Yao, C. Zawadzki, J. Bauer, M. Bauer, C. Dreyer, and J. Schneider, "Athermal all-polymer arrayed-waveguide grating multiplexer," Electron. Lett. **37,** 579–580 (2001).